Korean J. Chem. Eng., 40(7), 1650-1660 (2023)
DOI: 10.1007/s11814-022-1373-z

pISSN: 0256-1115
eISSN: 1975-7220

Enhanced adsorption of cationic and anionic dyes using cigarette butt-based adsorbents: Insights into mechanism, kinetics, isotherms, and thermodynamics

Thi Kieu Ngan Tran[*], Van Thuan Le[*,], Tien Hoang Nguyen[***], Van Dat Doan[****,†], Yasser Vasseghian[*****,******,*******,†], and Hoang Sinh Le[********,†]**

*The Faculty of Environmental and Natural Sciences, Duy Tan University, 03 Quang Trung, Da Nang, 550000, Viet Nam
**Center for Advanced Chemistry, Institute of Research and Development, Duy Tan University, 03 Quang Trung, Da Nang, 550000, Viet Nam
***The University of Da Nang, University of Science and Education, 459 Ton Duc Thang st., Lien Chieu, Da Nang 550000, Viet Nam
****Faculty of Chemical Engineering, Industrial University of Ho Chi Minh City, Ho Chi Minh City, Viet Nam
*****Department of Chemistry, Soongsil University, Seoul 06978, South Korea
******University Centre for Research & Development, Department of Mechanical Engineering, Chandigarh University, Gharuan, Mohali, Punjab, 140413, India
*******School of Engineering, Lebanese American University, Byblos, Lebanon
********VN-UK Institute for Research and Executive Education, University of Danang, Danang City 550000, Viet Nam
(*Received 2 November 2022 • Revised 3 December 2022 • Accepted 11 December 2022*)

Abstract−The present study provides an eco-friendly and economical way to recycle discarded cigarette butts (CBs). The raw CBs were treated with NaOH (CB-B) and integrated with chitosan (Cs), and further applied as an adsorbent for the removal of synthetic dyes. Two common cationic dyes of methylene blue (MB) and crystal violet (CV) and one anionic dye of reactive blue 19 (RB 19) were selected as model adsorbates. The study results revealed that CB-B showed a high adsorption ability toward cationic dyes, while the CB-B/Cs composite exhibited a stronger affinity for the anionic RB 19. The adsorption of all selected dyes onto CB-B and CB-B/Cs was a spontaneous exothermic process, conforming to the pseudo-first-order kinetic and Langmuir isotherm models. The maximum adsorption capacities for MB, CV and RB 19 at pH of 7, an adsorbent dosage of 4, and a temperature of 25 °C were 89.85, 82.41, and 304.49 mg/g, respectively. The primary adsorption mechanism was physical adsorption with the participation of electrostatic attraction. The CB-based adsorbents displayed high reusability, maintaining more than 75% after four consecutive cycles of reuse. This study demonstrates the promising application potential of CB-based adsorbents for treating synthetic dyes in wastewater. The conversion of CBs into a useful high-value material has special significance for environmental engineering.

Keywords: Cigarette Butts, Chitosan, Adsorption, Dye Removal, Water Treatment

INTRODUCTION

The deterioration of water quality due to pollution from industrial activity is a major concern worldwide [1]. Textile industries are considerable contributors to water pollution because they regularly discharge a large amount of highly colored wastewater [2]. Dye-containing wastewater seriously threatens human, animal and plant health and the environment due to its highly toxic nature. The presence of synthetic dyes in water can reduce photosynthesis, increase biochemical and chemical oxygen requirements, and inhibit the growth of aquatic organisms. They also can enter the food chain and accumulate in the body, and have the potential to promote toxicity, mutagenicity and carcinogenicity [3]. Therefore, dye effluents should be effectively treated before being discharged into water sources to avoid adverse effects on the environment and human health.

Among various technologies (membrane filtration, coagulation/flocculation, chemical oxidation, biological treatment, and photocatalysis) developed for the removal of dye-containing effluents, adsorption is one of the most efficient and economical methods due to its simplicity and high efficiency, selectivity, recycling facility, and the availability of a wide variety of adsorbents [4]. Several adsorbents, including activated carbon, zeolite, graphene, metal-organic frameworks, metal oxide-based, and polymer-based materials, have been extensively studied for the treatment of dye-contaminated water because they possess many advantages of large surface area, high adsorption capacity, and easy modification [5]. However, the complexity of synthesis and the high cost of these materials have limited their wide application. In recent years, the utilization of available natural resources, biomass, and agricultural and industrial wastes as non-conventional adsorbents in water treatment has emerged

†To whom correspondence should be addressed.
E-mail: doanvandat@iuh.edu.vn, vasseghian@ssu.ac.kr, sinh.le@vnuk.edu.vn

as a potential economic alternative to costly materials owing to their low cost, abundance, and effective adsorption capacity [6]. Various waste materials to adsorb toxic dyes from wastewater have been reported, such as spent coffee grounds and spent green tea leaves [7], sawdust [8], pomelo peel [9], *Eichhornia crassipes* and *Phragmites australis* stems [10].

Cigarette butts (CBs) are one of the most common forms of solid waste in the world. The annual amount of CB discarded worldwide is estimated at 5.6 trillion—a number that is growing every year [11]. The main constituent material of CBs is cellulose acetate, which does not biodegrade easily [12]. Besides, thousands of harmful substances (e.g., polycyclic aromatic hydrocarbons, pyridines, phenols, etc.) trapped in the CB during cigarette combustion can be easily leached out by the water, causing great harm to aquatic ecosystems and human health [13]. Therefore, it is urgent and meaningful to explore suitable methods for waste CBs reclamation. Some studies have attempted to convert CBs into valuable products, such as turning CBs into a mosquito repellant insecticide [14], integrating CB into building materials such as fired clay bricks [15], and converting into carbon-based catalysts [16,17], and supercapacitors [18].

Recently, extensive efforts have been made to transform CB effectively into activated carbon-based adsorbents for treating heavy metals and dye-containing wastewater. For example, Zhang et al. reported an effective way to convert discarded CBs into carbonaceous adsorbents for heavy metal removal from water [19]. Herein, the CBs were first hydrothermally heated in an autoclave with water at 250 °C for 2 h, followed by activation with KOH at 400-600 °C for 1 h. The resulting products demonstrated high adsorption capacity (up to 249.3 mg/g) for Cr^{3+}, Co^{2+}, Ni^{2+}, Cd^{2+}, and Pb^{2+}. Hamzah and Umar applied the microwave-induced KOH activation method to prepare activated carbon from CBs, which achieved a maximum adsorption capacity of 88.76 m^2/g towards methylene blue (MB) [20]. Converting BCs to activated carbon can improve their adsorption capacity; however, there are also the disadvantages of being energy and time-consuming, and a complex synthesis process. Unfortunately, using raw CBs is ineffective due to the low adsorption efficiency. The modification or combination with some other ingredients to create a composite is considered a promising way to create materials with superior adsorption properties.

Chitosan (Cs) is a kind of natural polysaccharide prepared predominantly through the deacetylation of chitin from crustacean shells [21]. In addition to applications in pharmaceuticals, medicine, pulp and paper, food, agriculture, textiles, cosmetics, and biotechnology, Cs is also known as an excellent adsorbent for the removal of heavy metals and dyes due to its naturally abundant sources, eco-friendliness, high adsorption efficiency and ease of modification [22]. Since Cs is less stable in hard acids and bases, for adsorption application, it is often cross-linked [23] or combined with other polymers such as cellulose [24] and alginate [25].

In this study, a simple, highly efficient, and low-cost approach to recycling CBs waste as adsorbents for synthetic dye removal was developed. Herein, the unused CBs were pretreated with NaOH and combined with Cs to form a composite adsorbent. The base treatment was performed to convert cellulose acetate to cellulose with more hydroxyl groups, which can promote the adsorption of cationic dyes. Meanwhile, the combination with Cs was to increase the adsorption capacity for anionic dyes. The prepared adsorbents were analyzed by X-ray diffraction (XRD) analysis, Fourier transform infrared reflectance (FTIR) spectroscopy, high-resolution scanning electron microscopy (SEM), and the Bruner-Emmett-Teller method. The adsorption behavior of the CBs-based adsorbents was tested with MB, crystal violet (CV), and reactive blue 19 (RB 19). The effects of adsorption factors such as contact time, initial pH, adsorbent dose, and initial dye concentration on dye adsorption were systematically investigated. The adsorption isotherms, kinetic and thermodynamic behaviors were established. The results indicated that the NaOH-treated CBs exhibited excellent adsorption ability toward cationic dyes (MB and CV), while the NaOH-CBs-Cs composite showed a stronger affinity for the anionic RB 19 dye.

MATERIALS AND METHODS

1. Materials and Chemicals

Unused CBs were collected from coffee bars in Danang City, Vietnam. All the reagents used in this study were of analytical grade. Hydrochloric acid (HCl, 35%), sodium hydroxide (NaOH, ≥98%), chitosan (percentage of deacetylation: 75%) and ethanol were purchased from Sigma-Aldrich. Methylene blue (MB, ≥70%), crystal

Table 1. The physical characteristics of MB, CV, and RB 19

Dye	Methylene blue	Crystal violet	Reactive blue 19
Structure	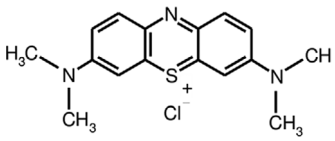	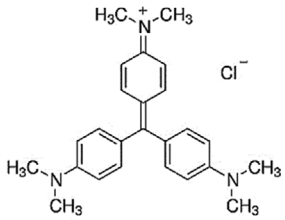	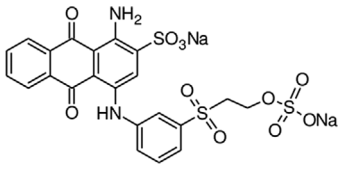
Chemical formula	$C_{16}H_{18}ClN_3S$	$C_{25}H_{30}ClN_3$	$C_{22}H_{16}O_{11}N_2S_3Na_2$
Type of dye	Cationic	Cationic	Anionic
Molar mass (g/mol)	319.85	407.98	626.5
Maximum wavelength (nm)	664	584	592

violet (CV, 98%) and reactive blue 19 (RB 19, 50%) dyes were purchased from Shanghai Aladdin Bio-Chem Technology Co., Ltd. (Shanghai, China) and used without purification. A stock dye solution of 1,000 mg/L was prepared by dissolving weighed amounts of dyes. The desirable experiments concentrations of solutions were prepared by diluting the stock solution with distilled water. The main physical characteristics of the used dyes are summarized in Table 1.

2. Absorbent Preparation

2-1. Preparation of CB Adsorbents

Firstly, the wrapping paper was removed from the CBs by soaking it in water. The unwrapped CBs were then cut into pieces about 1 mm, followed by washing many times with hot distilled water and then with alcohol. The dried CBs were ground into a fine powder using a pestle and mortar and then passed through a sieve of 100 mesh. The CB powder was further treated with HCl and NaOH, denoted as CB-A and CB-B, respectively.

The CB-A and CB-B samples were prepared according to the following procedure. Firstly, 20 g of the CB powder was soaked with 900 mL of 5% HCl or 5% NaOH solution (using absolute alcohol as solvent) at 60 °C for 4 h under continuous stirring. The treated samples were filtered and washed with distilled water to neutral pH. Finally, the products were dried at 60 °C overnight.

2-2. Preparation of CB-B/Cs Composite

Firstly, 1 g of Cs was dissolved in 50 mL of 2% CH_3COOH solution. Then, a calculated amount of CB-B was added to the Cs solution and stirred continuously for 1 h. The resulting mixture was soaked in 5% sodium tripolyphosphate solution for 5 h to create cross-linking for Cs with the aim of increasing the stability of the composite. The product was then filtered, washed with distilled water until pH neutral and dried at 60 °C overnight.

3. Adsorbent Characterization

The morphology features were obtained on a Hitachi S-4800 High-resolution scanning electron (SEM) (Hitachi, Japan). The surface area and pore size distribution of the adsorbents were determined using N_2 adsorption-desorption isotherms from the Bruner-Emmett-Teller method conducted on a Microactive Tristar II Plus analyzer (Micromeritics, USA) at 77 K. Fourier transform infrared (FTIR) spectroscopy analysis was performed on a Nicolet 6700 FT-IR spectrometer (Thermo Fisher Scientific, USA) in the wavelength of 4,000-500 cm^{-1} (resolution: 2 cm^{-1}, 64 scans). The X-ray diffraction (XRD) patterns were recorded on an Ultima IV X-ray diffractometer (Rigaku, Japan) with monochromatized Cu-Kα radiation (λ=0.15418 nm) at 40 kV, 30 mA and a scanning rate of 2θ= 0.02°.

The point of zero charge (PZC) of the synthesized adsorbents was determined by the salt addition method. Briefly, 0.01 g of the materials was added to 50 mL beakers containing 25 mL 0.01 M KCl with pH values in the range of 2-11. The initial pH of the solutions (pH_i) was adjusted by 0.1 M NaOH and 0.1 M HCl solutions and measured by a pH meter (Inolab multi 9310, Germany). The mixtures were shaken for 24 h at room temperature, and then the final pH (pH_f) was measured. The PZC was obtained after plotting a graph of $\Delta pH=pH_f-pH_i$ versus initial pH_i values. The pH_{ZPC} of the adsorbent was defined as the pH_i value at which ΔpH was equal to zero.

4. Adsorption Experiments

The adsorption of dyes on the CB-based adsorbents was investigated by the bath technique with different pH, contact time, initial concentration, adsorbent dosage, and temperatures. Typically, the adsorption experiments were carried out in a 50 mL centrifuge tube containing 25 mL of dye solutions of desired initial concentrations. The tubes were shaken on an oval shaker with a thermal stabilization system. After adsorption, the adsorbent was separated by centrifugation at 5,000 rpm for 10 min. The concentration of MB, CV, and RB 19 was measured using a Cary 60 UV-Vis spectrophotometer (Agilent, USA) at a wavelength of 664 nm, 584 nm, and 592 nm, respectively. All experiments were conducted in triplicates, and the absorbents after adsorption were collected for regeneration and reutilization. The adsorption kinetics was investigated by determining the adsorption capacity at different time intervals (2-60 min). The effect of pH on the dye adsorption was studied over a pH range of 3-9, adjusting by 0.1 M HCl or 0.1 M NaOH solutions before the adsorption experiments were performed. The effect of temperature was examined at 25, 35, 45 and 55 °C. The adsorption isotherms were determined by measuring the adsorption capacity of the material at different concentrations and then fitting it with common isotherm models.

The Eqs. (1) and (2) were used for calculating the removal efficiency (R, %) and adsorption capacity (q_e, mg/g) of the adsorbents.

$$R\% = \frac{C_0 - C_e}{C_0} \quad (1)$$

$$q_e = \frac{C_0 - C_e}{m} \times V \quad (2)$$

where C_o is the initial concentration of the dyes before adsorption (mg/L); C_e is the dye concentration after adsorption (mg/L); q_e is amount of adsorbate adsorbed at equilibrium time (mg/g); V is the volume of dye solution (L); and m is the mass of adsorbent (g).

RESULTS AND DISCUSSION

1. Preliminary Experiments

To select the suitable adsorbent, exploratory adsorption experiments were conducted. The raw CB after treatment with acid/base was tested for adsorption ability towards MB, CV, and RB 19 dyes. MB and CV are two cationic dyes widely used in ink and paper industries as well as in the dyeing of silk, cotton, and leather. These cationic dyes are considered more toxic than anionic ones. RB 19 is a typical anionic dye commonly used in the textile industry. With the presence of electrophonic vinyl sulfone groups in its structure, RB 19 can cause mutations in humans and animals when exposed to high concentrations. Thus, these dyes were chosen as anionic- and cationic-simulated dyeing effluents in this study.

The removal efficiencies of CB, CB-A, CB-B, and CB-B/Cs composite toward MB, CV, and RB 19 are shown in Fig. 1(a). It can be seen that the raw CB exhibited relatively low adsorption efficiency for all dyes, reaching only 41.67, 4.98, and 26.02% for MB, CV, and RB 19, respectively. After treatment with HCl and NaOH, the adsorption performance of CB for MB and CV was significantly

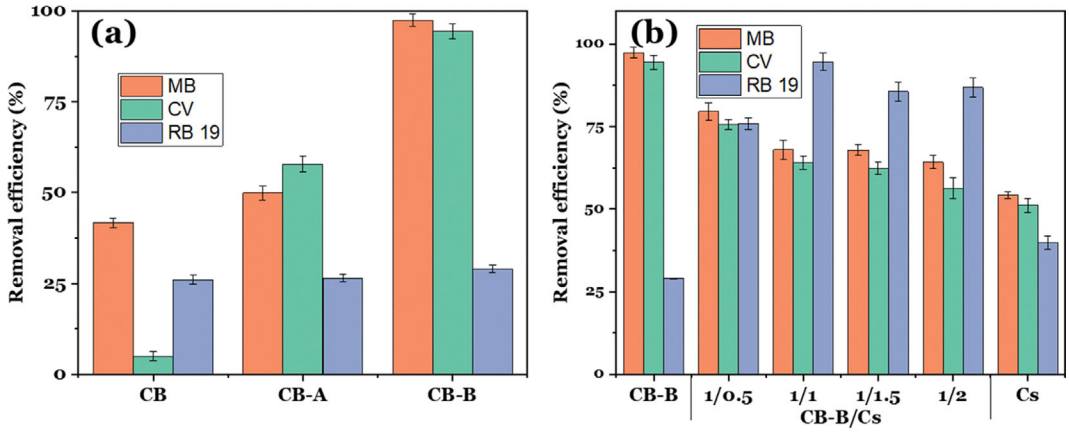

Fig. 1. Removal efficiency for MB, CV, and RB 19 dyes by (a) CB, CB-A, and CB-B, and (b) by CB-B/Cs composite with different mass ratio. Experiment conditions: pH=7, [dye]=20 mg/L, adsorbent dosage of 4 g/L, temperature of 25 °C, contact time of 60 min.

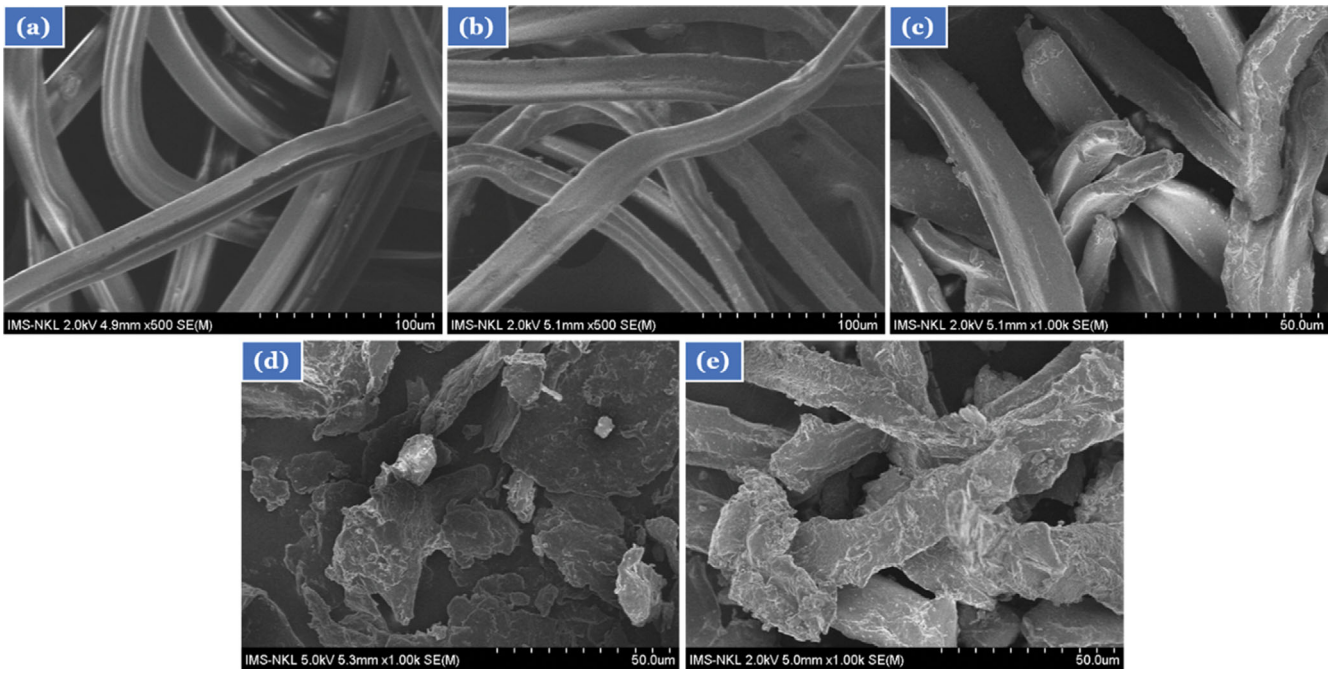

Fig. 2. SEM micrographs of the raw (a) CBs, (b) CB-A, (c) CB-B, (d) Cs, and (e) CB-B/Cs samples.

improved, especially for the CV dye. Meanwhile, RB 19 was very poorly absorbed by CB, CB-A and CB-B, with a removal efficiency of about 26%. In addition, the results also show that the CB-B sample processed the ability to adsorb MB (97.43%) and CV (94.44%) nearly 2 times higher than that of CB-A (49.92% for MB and 57.89% for CV), demonstrating the superiority of NaOH treatment. This can be associated with the fact that upon treatment with NaOH, the cellulose acetate in CB was converted to cellulose with an abundance of negatively charged OH groups, facilitating the adsorption of cationic dyes through electrostatic attraction.

Based on the results above, CB-B was selected to combine with Cs to create the composite adsorbent. The adsorption efficiency of the composites with different CB-B/Cs ratios is shown in Fig. 1(b). Obviously, introducing Cs to CB-B reduced the MB and CV adsorption. The decrease was more pronounced when increasing the Cs content in the composite. This phenomenon may be related to the decrease in the negative charge density of CB-B due to neutralization by the NH_3^+ group (protonated from the amine group $-NH_2$) from Cs. Many studies have indicated that Cs shows good adsorption efficiency to remove anionic contaminants through electrostatic attraction [24]. That is the cause of the significant increase in the adsorption of the anionic RB 19 dye when CB-B was combined with Cs. The removal efficiency of the composite for RB 19 increased 2-3 times compared with pure CB-B and Cs. The synergistic effect between Cs and cellulose resulted in a high adsorption performance for the prepared composite, as indicated in previous studies [26-28]. The CB-B/Cs sample with a ratio of 1 : 1 showed the highest removal efficiency for RB 19 (94.34%). With further increasing the mass ratio between CB-B and Cs to 1 : 1.5 and 1 : 2, the adsorption rate of RB 19 decreased slightly to about 85%. There-

fore, the CB-B/Cs composite with a weight ratio of 1 : 1 was chosen for the RB 19 adsorption. Meanwhile, CB-B was used for the adsorption of MB and CV.

2. Characterization of Adsorbents

The morphology of the prepared samples was examined by SEM, and the results are presented in Fig. 2. It can be seen in Fig. 2(a) that the untreated CBs sample are long smooth fibers with a diameter of about 20 μm. Treatment with acid caused slight damage to the surface of cellulose acetate fibers, but in general, their morphology was almost unchanged (Fig. 2(b)). As shown in Fig. 2(c), the CB fibers were cut shorter, and their surface became rougher after treatment with NaOH, which benefited dye absorption. The pure Cs presented as thin flakes with a size of 10-100 μm (Fig. 2(d)). Meanwhile, the CB-B/Cs composite revealed porous fiber structures with a rough Cs-coated surface.

Fig. 3(a) displays the XRD spectra of individual CB, CB-B, Cs, and CB-B/Cs samples, recorded in a 2θ range of 10-70°. The XRD spectrum of CB showed two peaks around 2θ=22.1° and 2θ=28.3°, corresponding to the cellulose acetate structure [29]. The diffraction peaks at 2θ=12.3°, 19.9°, 21.8°, 25.4° and 26.7° appeared in the XRD pattern of CB-B were ascribed to the cellulose phase [30]. Meanwhile, the Cs sample illustrated the board diffraction peak at 2θ=20.2°, typical for hydrophilic Cs crystalline lattice [31]. The CB-B/Cs composite showed all characteristic peaks of CB-B and Cs. Notably, the typical peaks for CB-B in the prepared composite were of lower intensity than those of the individual CB-B, possibly due to the occlusion of Cs.

The FTIR analysis was carried out to establish the functional groups of the synthesized adsorbents. As depicted in Fig. 3(b), the spectrum of the untreated CB sample containing cellulose acetate fiber exhibited characteristic bands at 3,496, 1,735, 1,215, and 1,033 cm^{-1} assigned to the hydroxyl group (-OH), carbonyl group (C=O), acetyl ester group (CH_3-C=O), and ether group (C-O-C), respectively [32]. The peaks at 2,954 and 2,887 cm^{-1} were attributed to the symmetric and asymmetric stretching of methyl group (C-H), respectively. The bands at 1,430 and 1,368 cm^{-1} can be assigned to -CH_2 bending [29]. The spectrum of CB-B was almost similar to that of CB. A sharp decrease in the intensity of the typical carbonyl (at 1,735 cm^{-1}) and acetyl ester (1,215 cm^{-1}) stretching bands of the acetate group, as well as an increase in the intensity of the O-H group (3,319 cm^{-1}) in the CB-B sample, demonstrated the successful conversion of cellulose acetate to cellulose. In the case of pure Cs, the characteristic groups of Cs such as hydroxyl (O-H), methyl (C-H), carbonyl (C-O) in the acylamino group, and methoxy (-C-O-) groups were observed at 3,345, 2,882, 1,644, and 893-1,025 cm^{-1}, respectively. The bands at 3,345, 1,585, and 1,314-1,417 cm^{-1} were

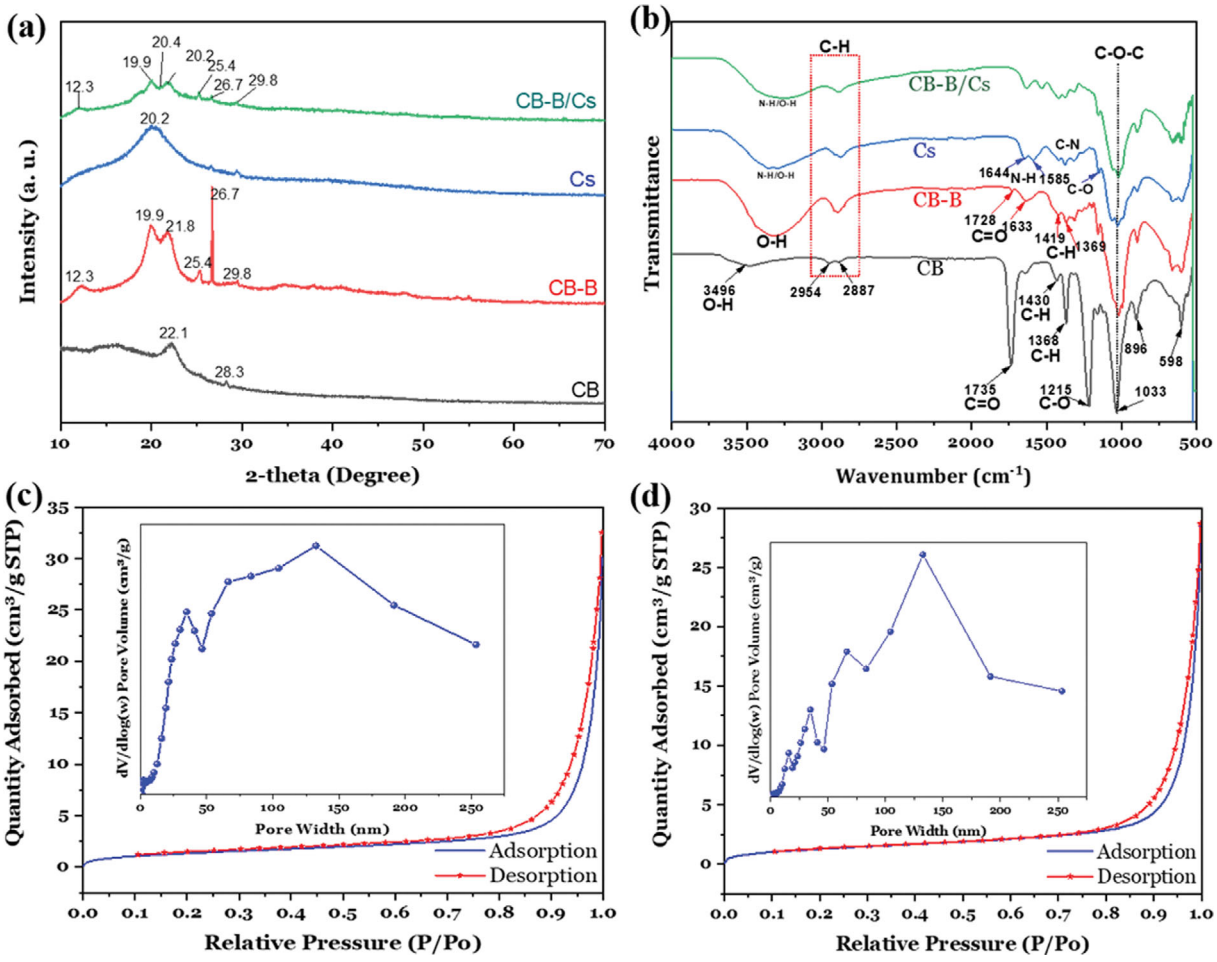

Fig. 3. (a) XRD patents, (b) FTIR spectra, (c) N_2 adsorption-desorption isotherms of CB-B, and (d) CB-B/Cs (1 : 1).

attributed to the stretching vibration of N-H amide, the bending vibration of N-H amide, and the stretching vibration of C-N amine I, respectively [24]. All the characteristic peaks for CB-B and Cs were found in the FTIR spectrum of the composite. Consequently, the SEM, FTIR and XRD analyses suggested that Cs was successfully coated on the CB-B fibers.

The texture properties of the synthesized adsorbents were analyzed based on the nitrogen adsorption-desorption data using the BET equation. Fig. 3(c) and Fig. 3(d) show the N_2 adsorption-desorption isotherms and the corresponding pore size distributions (insets) for CB-B and CB-B/Cs, respectively. It can be seen that both samples showed type-IV isotherms according to the IUPAC classification. In addition, the isotherms exhibited a very narrow hysteresis loop in the relative pressure (P/P_0) range of 0.4-1.0, indicating that the prepared adsorbents were mesoporous materials with a typical less-pore structure [33]. The BET-specific surface area of CB-B and CB-B/Cs was calculated to be 6.6 and 4.5 m^2/g, respectively. It can be noticed that the coating of Cs on the surface of CB-B led to a decrease in the specific surface area. The pore size distributions (insets in Fig. 3(c) &(d)) confirmed that the fabricated materials possessed mesopores and macropores with a maximum pore diameter of ~30 and 135 nm, respectively.

3. Effect of pH

The initial pH of the adsorption system is one of the most important factors that has a great influence on the surface charge of adsorbent and dye molecules, and thereafter affecting the adsorption capability of the adsorbent. The effects of pH on the adsorption of MB, CV and RB 19 were studied in the range of 3-9, as shown in Fig. 4(a). In general, the adsorption of MB and CV on CB-B increased with increasing pH. The removal rate of these dyes increased rapidly with increasing pH from 5 to 7, then barely increased. Meanwhile, the removal of RB 19 by CB-B/Cs showed the opposite variation trends. The adsorption behavior of the dyes at different pH can be explained through pH_{pzc} as follows. It is well known that the net charge of the adsorbent surface is positive when the pH of the solution is lower than pH_{pzc} and vice versa. As depicted in Fig. 4(b), the pH_{pzc} of CB and CB/Cs was found to be 5.1 and 6.5, respectively. The CB sample was positively charged when pH<5.1, which was unfavorable for the adsorption of cationic dyes due to electrostatic repulsion. When the pH grew higher (>5.1), the surface of CB became negatively charged and facilitated the adsorption of MB and CV. For the case of the anionic RB 19, the adsorption at low pH (<6.5) was more favorable than at higher pH due to the electrostatic attraction between the positively charged CB-B/Cs surface and the RB 19. Similar results have been reported for other adsorbents [24,29,34].

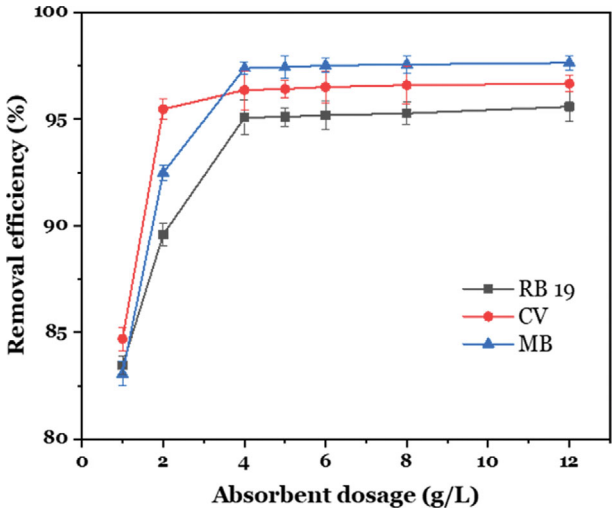

Fig. 5. Effect of CB-B and CB-B/Cs dosage on the adsorption of MB, CV and RB 19. Experiment conditions: pH=7, [dye]= 75 mg/L, temperature of 25 °C, contact time of 60 min.

4. Effect of Adsorbent Dosage

The effect of adsorbent dosage on dye adsorption was investigated to select the suitable adsorbent dosage for real application. The adsorption experiments were conducted by varying dosage from 1 to 12 g/L, and the obtained results are depicted in Fig. 5. Generally, the removal efficiency of dyes increased with increasing adsorbent dose due to the increased number of adsorption sites. However,

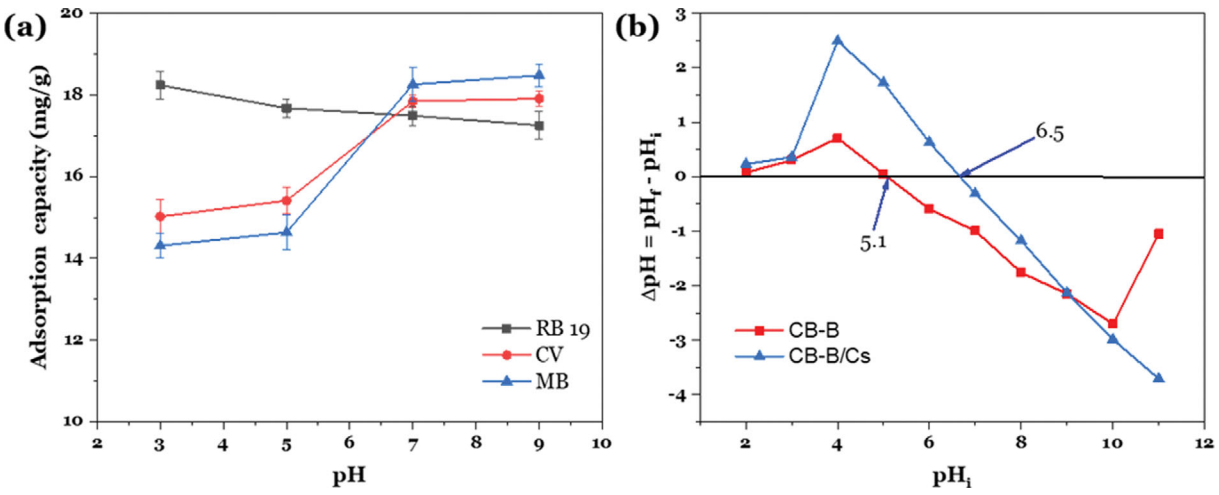

Fig. 4. Effect of (a) pH and (b) pH_{PZC} of CB-B and CB-B/Cs. Adsorption conditions: Adsorbent dosage of 4 g/L, [dye]=75 mg/L, temperature of 25 °C, contact time of 60 min.

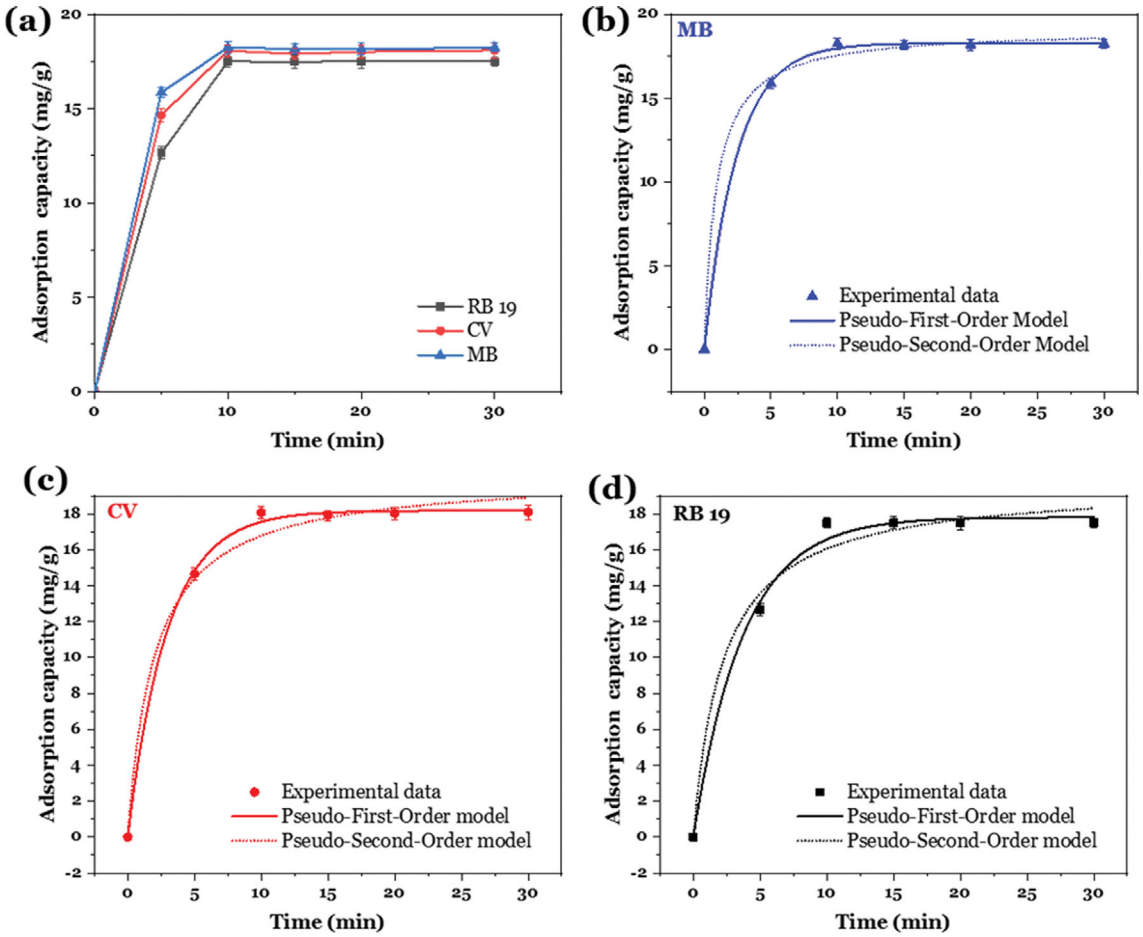

Fig. 6. Effect of (a) contact time, (b) non-linear fitting of PFO and PSO for the adsorption of MB, (c) CV, and (d) RB 19. Experiment conditions: pH=7, [dye]=75 mg/L, temperature of 25 °C, adsorbent dosage of 4 g/L.

when the amount of adsorbent was excess, the adsorption efficiency did not increase anymore [35]. The adsorption of MB, CV and RB 19 increased rapidly from 83.1, 84.7, and 82.9% to 97.4, 96.3, and 95.1%, with rising the amount of adsorbent from 1 to 4 g/L, respectively, and then it increased almost insignificantly. The saturation in percentage removal of the dyes at high adsorbent concentrations may be due to the redundancy of the adsorption sites and their mutual shielding. Therefore, the optimum adsorbent dosage was selected to be 4 g/L for further experiments.

5. Effect of Contact Time and Adsorption Kinetics

The time required for reaching adsorption equilibrium was established by monitoring the adsorption rate over time. As shown in Fig. 6(a), the adsorption of all dyes took place rapidly at the first 5 min, then slowly at the next 5 min, and reached the equilibrium state after 10 min. The fast adsorption rate in the first stage was assigned to the abundance of accessible sites. In the next stage, the adsorption driving force gradually decreased as the difference between the dye concentration and the adsorbent surface reduced, weakening the adsorption rate [24]. Generally, the adsorption of MB, CV, and RB 19 onto CB-B and CB-B/Cs is quite fast, which is one of the characteristics of physical adsorption.

To explore the adsorption kinetics of CB-B toward CV and MB and CB-B/Cs toward RB 19, two common adsorption kinetic models, including pseudo-first-order (PFO, Eq. (3)) and pseudo-second-order (PSO, Eq. (4)), were used to analyze the experimental data. The non-linear fitting of PFO and PSO for the adsorption of MB, CV, and RB 19 is illustrated in Fig. 6(b)-(d). The corresponding calculated parameters are summarized in Table 2.

$$q_t = q_e(1 - e^{-k_1 t}) \quad (3)$$

$$q_t = \frac{q_e^2 k_2 t}{1 + q_e k_2 t} \quad (4)$$

Table 2. Kinetic parameters for the MB, CV, and RB 19 adsorption

Adsorption kinetic model	MB	CV	RB 19
$q_{e,exp}$ (mg/g)	18.23	18.09	17.49
PFO model			
$q_{e,cal}$ (mg/g)	18.27	18.17	17.81
k_1 (1/min)	0.411	0.338	0.267
R^2	0.999	0.9987	0.995
PSO mode			
q_{cal} (mg/g)	19.13	20.16	19.67
K_2 [g/(mg.min)]	0.058	0.025	0.023
R^2	0.997	0.972	0.985

where q_t and q_e (mg/g) are the adsorption capacity of the adsorbent at time t (min) and equilibrium, respectively; k_1 (1/min) and k_2 [g/(mg·min)] are the rate constants of PFO and PSO, respectively.

It is observed from Fig. 4(b)-(d) that the PFO kinetic model showed a better fit to the adsorption data than the PSO. This is also confirmed by the results given in Table 2. The correlation coefficients (R^2) for MB, CV, and RB 19 from PFO were calculated as 0.999, 0.9987, and 0.995, respectively, which are higher than those from PSO. Besides, the equilibrium adsorption capacities ($q_{e,cal}$) calculated by PFO were closer to the experimental adsorption values ($q_{e,exp}$). These findings indicated that the adsorption of CV and MB onto CB-B and RB 19 onto CB-B/Cs can be best predicted by the PFO equation.

6. Adsorption Isotherms

The adsorption isotherm is a mathematical model that describes the relationship between the adsorbate amount adsorbed on the

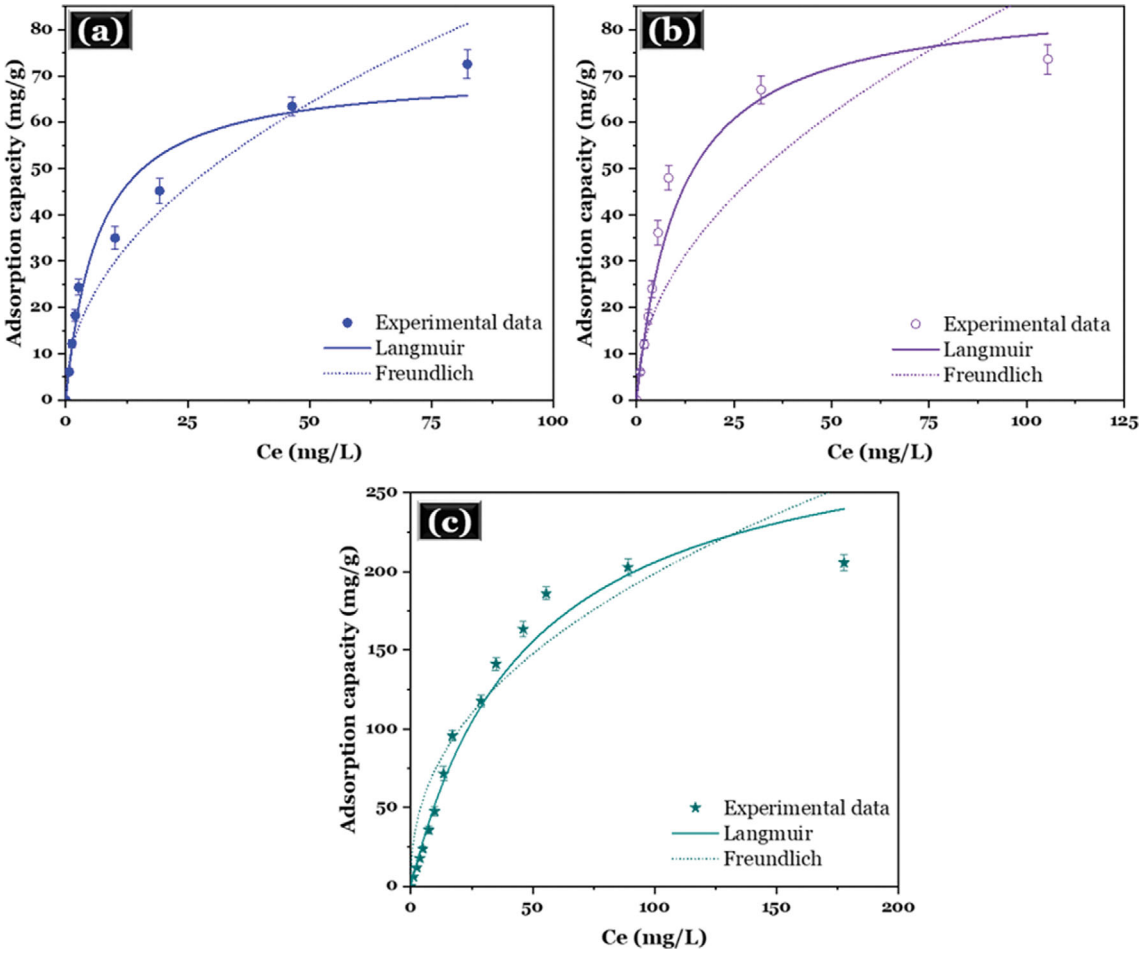

Fig. 7. Non-linear fitting of the (a) Langmuir and Freundlich models for the adsorption of MB, (b) CV, and (c) RB 19 at 25 °C. Experiment conditions: pH=7, contact time of 20 min, temperature of 25 °C, adsorbent dosage of 4 g/L.

Table 3. Parameters of isothermal models for the adsorption of MB, CV, and RB 19 into CB-B and CB-B/Cs at 25, 35 and 45 °C

Isotherm model	25 °C			35 °C			45 °C		
	MB	CV	RB 19	MB	CV	RB 19	MB	CV	RB 19
Langmuir									
q_m (mg/g)	89.85	82.41	304.49	80.78	77.97	236.17	76.05	74.31	211.49
K_L (L/mg)	0.15	0.13	0.07	0.12	0.10	0.05	0.09	0.08	0.04
R^2	0.979	0.974	0.981	0.992	0.975	0.978	0.984	0.972	0.978
Freundlich									
K_F [(mg/g)/(mg/L)^n]	15.64	19.04	27.61	12.88	15.68	19.05	10.23	13.71	16.51
n	0.48	0.49	0.43	0.39	0.34	0.47	0.43	0.35	0.47
R^2	0.951	0.834	0.971	0.986	0.876	0.889	0.976	0.867	0.891

Table 4. Thermodynamic parameters of MB, CV, and RB 19 adsorption onto CB based adsorbents

	T (K)	K_c	van't Hoff equation	ΔG (kJ/mol)	ΔH (kJ/mol)	ΔS (J/(mol·K))
MB	298	47,977	y=2416.2x+2.68	−26.69	−7.59	22.27
	308	38,382	R^2=0.9916	−27.02		
	318	28,786		−27.13		
CV	298	53,037	y=2301.6x+3.15	−26.94	−7.23	26.18
	308	40,798	R^2=0.9982	−27.17		
	318	32,638		−27.46		
RB 19	298	43,855	y=2656.4x+1.76	−26.47	−8.34	14.62
	308	31,325	R^2=0.9905	−26.50		
	318	25,060		−26.77		

adsorbent and the adsorbate in the liquid phase at the equilibrium state. In this study, Langmuir (Eq. (5)) and Freundlich (Eq. (6)) isotherm models were used to describe the adsorption isotherm data. The Langmuir isotherm confirms the mono-layer adsorption on the homogeneous surface of an adsorbent, while the Freundlich model explains the multilayer adsorption on the heterogeneous surface [36]. The non-linearly fitted curves for the adsorption of MB, CV and RB 19 on CB-B and CB-B/Cs at 25, 35 and 45 °C are presented in Fig. 7 and Fig. S1 (Supporting Information). The fitting adsorption parameters are listed in Table 3.

$$q_e = \frac{q_m \cdot K_L C_e}{1 + K_L C_e} \quad (5)$$

$$q_e = K_F \cdot C^n \quad (6)$$

where q_m (mg/g) is the maximum adsorption capacity; K_L (L/mg) and K_F [(mg/g)/(mg/L)^n] indicate the constant of the Langmuir and Freundlich models, respectively; n denotes adsorption intensity of adsorbent.

The results demonstrated that the Langmuir model with higher R^2 values at all temperatures was more suitable for describing the adsorption behavior of MB/CV onto CB-B and RB 19 onto CB-B/Cs compared with the Freundlich. This revealed that monolayer adsorption was the predominant adsorption mechanism. The maximum adsorption capacities calculated according to the Langmuir isotherm at 25 °C for MB, CV, and RB 19 were 89.85, 82.41, and 304.49 mg/g, respectively. Notably, the adsorption capacity values for all studied dyes decreased with increasing adsorption temperature (Table 3), indicating unfavorable adsorption at high temperatures. This phenomenon can be attributed to the increase in thermal motion of the dye molecules, which increased the desorption rate, diminishing the adsorption capacity of CB-B and CB-B/Cs. In addition, the adsorption performances of CB-B and CB-B/Cs were comparative or superior to that of other reported adsorbents (Table S1).

7. Adsorption Thermodynamics

The mechanism of the adsorption process (i.e., physical, or chemical) can be rationally explained through the study of adsorption thermodynamics. In this study, the thermodynamic parameters, including enthalpy change (ΔH, kJ/mol), entropy change (ΔS, J/(mol·K)), and the standard Gibbs free energy (ΔG, kJ/mol) were calculated using the van't Hoff approach (Eq. (7)-(9)).

$$\Delta G = -RT\ln K_c \quad (7)$$

$$K_c = K_L \cdot M \cdot C^o \cdot 1000 \quad (8)$$

$$\ln K_c = -\frac{\Delta H}{RT} + \frac{\Delta S}{R} \quad (9)$$

where K_c is the thermodynamic equilibrium constant (dimensionless); T is the absolute temperature (K); R is the universal gas constant (8.3144 J/(mol.K)); K_L is Langmuir constant (L/mg) (from Table 3); M is molar mass of dyes; C^o is the standard state using to change all concentration to molar form (C^o=1 mol/L); and 1000 is a factor for converting the units from gram to milligram [37].

Table 4 lists the thermodynamic parameters for the adsorption of MB, CV, and RB 19 onto CB-based adsorbents. The ΔH values for MB, CV, and RB 19 were relatively low and were found to be −7.59, −7.23, and −8.34 kJ/mol, respectively. The low (less than 20-40 kJ/mol) and negative values of ΔH reflected the physical and exothermic nature of the adsorption processes. Furthermore, the negative ΔG values at all investigated temperatures confirmed that the adsorption phenomenon occurred spontaneously. As well, a positive value of ΔS (14.62-22.27 J/(mol·K)) indicated the increased randomness of motion of dye molecules at the solid-solution interface during adsorption.

8. Possible Adsorption Mechanism

Adsorption is a complex process that can occur via one or a combination of mechanisms. The adsorption process can be divided into two types: physical adsorption and chemical adsorption. Physical adsorption is reversible and occurs rapidly at low temperatures with small adsorption energy. This adsorption category is produced by the interaction of intermolecular forces (i.e., van der Waals forces). In contrast, chemical adsorption arises from strong interactions with the existence of an endothermic process. It is not easy to understand the adsorption mechanism of an adsorbent with many functional groups. Based on the results of analyzing the characterization and adsorption behavior of CB-based adsorbents, the possible adsorption mechanism can be discussed as follows. The presence of the surface functional groups, including -COOH, -OH and -NH_2 in the CB-based adsorbents may provide the chemisorption for MB, CV and RB 19 by hydrogen bonding. However, the comparison of the FITR spectra of CB-B and CB-B/Cs before and after adsorption (Fig. S2, Supporting Information) showed that no significant difference was found, confirming the negligible contribution of hydrogen bonding in the adsorption process [38].

A wide range distribution of pore size of CB-B and CB-B/Cs

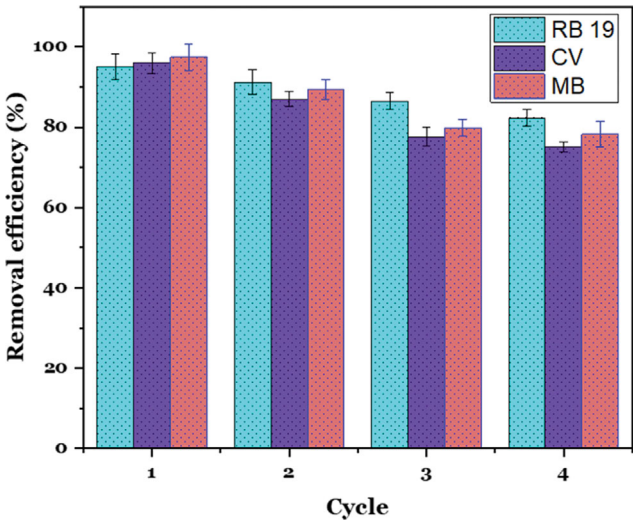

Fig. 8. Removal efficiency of CB-based adsorbents for MB, CV, and RB 19 in recycles. Experiment conditions: pH=7, contact time of 20 min, temperature of 25 °C, adsorbent dosage of 4 g/L.

(Fig. 3(c) & (d)) can be available for the physical adsorption of MB/CV and RB19 via the pore pilling mechanism. Meanwhile, the specific surface area of the prepared adsorbents was low (6.6 and 4.5 m^2/g for CB-B and CB-B/Cs, respectively), revealing that the surface diffusion did not give a significant contribution to the adsorption [34]. The study on the effect of pH confirmed that electrostatic attraction played a remarkable role in the adsorption process. Moreover, the results of the kinetic and thermodynamic analysis indicated that the adsorption of MB/CV and RB 19 onto CB-B and CB-B/Cs was fast and exothermic with low adsorption energy. All these findings support the conclusion that the adsorption process is physical.

9. Adsorption Reversibility

The reusability experiments were performed to evaluate the applicability of the CB-based adsorbents. Because the adsorption became lower for MB/CV and higher for RB 19 with increasing aqueous pH, as aforementioned in Section "Effect of pH", HCl and NaOH solutions were selected as eluent for the desorption of MB/CV and RB 19, respectively. After the first adsorption, the adsorbents were soaked 2 times with 50 mL 0.01 M HCl/NaOH at 60 °C for 1 h for desorption. Then, the adsorbents were dried and used for the next adsorption experiment. The reuse was repeated 4 times, as depicted in Fig. 8.

In general, the adsorption efficiency of all dyes decreased progressively with the number of repeated runs. This reduction may be related to the incomplete desorption and the abrasiveness of the adsorption sites. After two consecutive adsorption-desorption cycles, the adsorption efficiency of CB-based adsorbents for all dyes was higher than 85%; and after the 4th round of reuse, these values remained at 75, 78, and 82% for CV, MB, and RB 19, respectively. This result confirmed the good stability of the prepared adsorbents.

CONCLUSIONS

Discarded CBs were successfully recycled to fabricate adsorbents for removing synthetic dyes from aqueous solutions. Raw CBs were treated with HCl and NaOH and combined with Cs to improve adsorption properties. The results showed that the NaOH-treated CBs exhibited high adsorption capacity for cationic dyes (MB and CV), while the CB-C/Cs composite showed a stronger affinity toward the anionic RB 19 dye. The adsorption of cationic dyes on CB-B was favorable at pH≥7, while the anionic RB 19 dye was removed effectively by CB-B/Cs at pH≤7. The optimal dosage of CB-based adsorbents for the adsorption of both cationic and anionic dyes was determined as 4 g/L. The kinetic study verified a fast adsorption equilibrium at ~10 min, and the adsorption process was well described with the PFO model. Thermodynamics analysis confirmed spontaneous and exothermic adsorption. The Langmuir isotherm model well depicted the equilibrium adsorption of CB-B and CB-B/Cs toward both MB, CV, and RB 19, with maximum adsorption capacities of 89.85, 82.41, and 304.49 mg/g, respectively. The primary adsorption mechanism was physical adsorption. The recycling test revealed that the CB-based adsorbents could be reused several times with adsorption efficiency higher than 75% after four adsorption-desorption runs. The overall results demonstrated that CB-B and CB-B/Cs are potential absorbents for treating dye-containing wastewater due to their high adsorption capacity, low cost, and simple synthesis pathway. The present study provides an environmentally friendly and economical way for CB recycling.

ACKNOWLEDGEMENTS

This study was funded by Duy Tan University.

DECLARATION OF INTERESTS

The authors declare that they have no known competing financial interests or personal relationships that could have appeared to influence the work reported in this paper.

ABBREVIATIONS AND SYMBOLS

BET : Bruner-Emmett-Teller
CB-B : cigarette butts modified with NaOH
CBs : cigarette butts
Cs : chitosan
CV : crystal violet
FTIR : Fourier transform infrared reflectance spectroscopy
MB : methylene blue
PZC : point of zero charge
RB 19 : reactive blue 19
SEM : scanning electron microscopy
XRD : X-ray diffraction
C_e : concentration of dye at equilibrium [mg/L]
C_o : initial concentration of the dyes before adsorption [mg/L]
k_1 : rate constant of pseudo first order adsorption [1/mg]
k_2 : second-order rate constant of adsorption [g/(mg·min)]
K_c : thermodynamic equilibrium constant
K_F : Freundlich constant $[(mg/g)/(mg/L)^n]$
K_L : Langmuir constant [L/mg]
m : mass of adsorbent [g]

n : adsorption intensity of adsorbent
q_e : amount of adsorbate adsorbed at equilibrium [mg/g]
q_m : maximum adsorption capacity [mg/g]
q_t : adsorption capacity of the adsorbent at any time [mg/g]
R : universal gas constant [J/(mol·K)]
T : absolute temperature [K]
t : adsorption time [min]
V : volume of dye solution [L]
ΔG : Gibbs free energy change [kJ/mol]
ΔH : enthalpy change [kJ/mol]
ΔS : entropy change [J/(mol·K)]

SUPPORTING INFORMATION

Additional information as noted in the text. This information is available via the Internet at http://www.springer.com/chemistry/journal/11814.

REFERENCES

1. A. Hojjati-Najafabadi, M. Mansoorianfar, T. Liang, K. Shahin, Y. Wen, A. Bahrami, C. Karaman, N. Zare, H. Karimi-Maleh and Y. Vasseghian, *J. Water Process Eng.*, **47**, 102696 (2022).
2. Z. Li, Y. Xing, Y. Liu, A. Meng and X. Fan, *RSC Adv.*, **12**, 29878 (2022).
3. R. Al-Tohamy, S. S. Ali, F. Li, K. M. Okasha, Y. A.-G. Mahmoud, T. Elsamahy, H. Jiao, Y. Fu and J. Sun, *Ecotoxicol. Environ. Saf.*, **231**, 113160 (2022).
4. G. Suresh, B. Balasubramanian, N. Ravichandran, B. Ramesh, H. Kamyab, P. Velmurugan, G. V. Siva and A. V. Ravi, *Biomass Convers. Biorefinery*, **11**, 383 (2021).
5. S. Dutta, B. Gupta, S. K. Srivastava and A. K. Gupta, *Mater. Adv.*, **2**, 4497 (2021).
6. L. Rao, Y. Zhu, Z. Duan, T. Xue, X. Duan, Y. Wen, A. S. Kumar, W. Zhang, J. Xu and A. Hojjati-Najafabadi, *Chemosphere*, **301**, 134595 (2022).
7. T. Jóźwiak, U. Filipkowska, J. Struk-Sokołowska, K. Bryszewski, K. Trzciński, J. Kuźma and M. Ślimkowska, *Sci. Rep.*, **11**, 1 (2021).
8. R. Chikri, N. Elhadiri, M. Benchanaa and Y. El maguana, *J. Chem.*, **2020**, 8813420 (2020).
9. S. K. Low and M. C. Tan, *J. Environ. Chem. Eng.*, **6**, 3502 (2018).
10. V. Dat Doan, T. Kieu Ngan Tran, A.-T. Nguyen, V. Anh Tran, T. Duy Nguyen and V. Thuan Le, *Environ. Nanotechnol., Monit. Manag.*, **16**, 100569 (2021).
11. Y. Lyu, T. A. Asoh and H. Uyama, *ACS Omega*, **6**, 15374 (2021).
12. J. Zhang, H. Xu, J. Guo, T. Chen and H. Liu, *Appl. Sci.*, **10**, 1985 (2020).
13. M. Michael, A. Meyyazhagan, K. Velayudhannair, M. Pappuswamy, A. Maria, V. Xavier, B. Balasubramanian, R. Baskaran, H. Kamyab, Y. Vasseghian, S. Chelliapan, M. Safa, Z. Moradi and M. A. Khadimallah, *Sustainability*, **14**, 4752 (2022).
14. K. Murugan, U. Suresh, C. Panneerselvam, R. Rajaganesh, M. Roni, A. T. Aziz, J.-S. Hwang, K. Sathishkumar, A. Rajasekar, S. Kumar, A. A. Alarfaj, A. Higuchi and G. Benelli, *Environ. Sci. Pollut. Res.*, **25**, 10456 (2018).
15. H. Kurmus and A. Mohajerani, *Materials (Basel)*, **13**, 790 (2020).
16. U. Veerabagu, Z. Chen, J. Xiang, Z. Chen, M. Liu, H. Xia and F. Lu, *J. Environ. Chem. Eng.*, **9**, 105246 (2021).
17. X. Jin, Y. Hao, C. Liu, H. Feng, X. Li, Y. Zhu, Y. Zhou, Y. Song and J. Hu, *New J. Chem.*, **45**, 19358 (2021).
18. L. Li, C. Jia, X. Zhu and S. Zhang, *J. Clean. Prod.*, **256**, 120326 (2020).
19. X. Zhang, M. Yu, Y. Li, F. Cheng, Y. Liu, M. Gao, G. Liu, L. Hu and Y. Liang, *Microchem. J.*, **168**, 106474 (2021).
20. Y. Hamzah and L. Umar, *J. Phys. Conf. Ser.*, **853**, 012027 (2017).
21. T. T. N. Le, V. T. Le, M. U. Dao, Q. V. Nguyen, T. T. Vu, M. H. Nguyen, D. L. Tran and H. S. Le, *Chem. Eng. Commun.*, **206**, 1337 (2019).
22. N. Morin-Crini, E. Lichtfouse, G. Torri and G. Crini, *Environ. Chem. Lett.*, **17**, 1667 (2019).
23. L. Van Thuan, T. B. Chau, T. T. K. Ngan, T. X. Vu, D. D. Nguyen, M. H. Nguyen, D. T. T. Thao, N. To Hoai and L. H. Sinh, *Environ. Technol. (United Kingdom)*, **39**, 1745 (2018).
24. X. Xu, J. Yu, C. Liu, G. Yang, L. Shi and X. Zhuang, *React. Funct. Polym.*, **160**, 104840 (2021).
25. X. Zhao, X. Wang and T. Lou, *J. Hazard. Mater.*, **403**, 124054 (2021).
26. U. J. Kim, S. Kimura and M. Wada, *Carbohydr. Polym.*, **214**, 294 (2019).
27. B. Shetty, Y. S. R and J. Johns, *Res. Sq.*, **2022**, 1 (2022).
28. Y. Wang, H. Wang, H. Peng, Z. Wang, J. Wu and Z. Liu, *Fibers Polym.*, **19**, 340 (2018).
29. A. Tehrim, M. Dai, X. Wu, M. M. Umair, I. Ali, M. A. Amjed, R. Rong, S. F. Javaid and C. Peng, *J. Appl. Polym. Sci.*, **138**, 1 (2021).
30. X. Song, M. Wei, Y. He, X. Pan, X. Cui, X. Du and J. Li, *Appl. Sci.*, **12**, 12094196 (2022).
31. Rahmi, S. Lubis, N. Az-Zahra, K. Puspita and M. Iqhrammullah, *Int. J. Eng. Trans. B Appl.*, **34**, 1827 (2021).
32. E. Baladi, F. Davar and A. Hojjati-Najafabadi, *Environ. Res.*, **215**, 114270 (2022).
33. Z. Qi, H. Lan, T. P. Joshi, R. Liu, H. Liu and J. Qu, *RSC Adv.*, **6**, 66990 (2016).
34. C. Liang, Q. Shi, J. Feng, J. Yao, H. Huang and X. Xie, *Nanomaterials*, **12**, 1814 (2022).
35. V. T. Le, V. D. Doan, D. D. Nguyen, H. T. Nguyen, Q. P. Ngo, T. K. N. Tran and H. S. Le, *Water, Air, Soil Pollut.*, **229**, 101 (2018).
36. Z. Esmaeili, S. Izadyar, Y. Hamzeh and A. Abdulkhani, *J. Chem. Eng. Data*, **66**, 1068 (2021).
37. M. U. Dao, H. S. Le, H. Y. Hoang, V. A. Tran, V. D. Doan, T. T. N. Le, A. Sirotkin and V. T. Le, *Environ. Res.*, **198**, 110481 (2021).
38. C. C. Fu, H. N. Tran, X. H. Chen and R. S. Juang, *J. Ind. Eng. Chem.*, **83**, 235 (2020).

Supporting Information

Enhanced adsorption of cationic and anionic dyes using cigarette butt-based adsorbents: Insights into mechanism, kinetics, isotherms, and thermodynamics

Thi Kieu Ngan Tran[*], Van Thuan Le[*,], Tien Hoang Nguyen[***], Van Dat Doan[****,†], Yasser Vasseghian[*****,******,*******,†], and Hoang Sinh Le[********,†]**

*The Faculty of Environmental and Natural Sciences, Duy Tan University, 03 Quang Trung, Da Nang, 550000, Viet Nam
**Center for Advanced Chemistry, Institute of Research and Development, Duy Tan University, 03 Quang Trung, Da Nang, 550000, Viet Nam
***The University of Da Nang, University of Science and Education, 459 Ton Duc Thang st., Lien Chieu, Da Nang 550000, Viet Nam
****Faculty of Chemical Engineering, Industrial University of Ho Chi Minh City, Ho Chi Minh City, Viet Nam
*****Department of Chemistry, Soongsil University, Seoul 06978, South Korea
******University Centre for Research & Development, Department of Mechanical Engineering, Chandigarh University, Gharuan, Mohali, Punjab, 140413, India
*******School of Engineering, Lebanese American University, Byblos, Lebanon
********VN-UK Institute for Research and Executive Education, University of Danang, Danang City 550000, Viet Nam
(*Received 2 November 2022 • Revised 3 December 2022 • Accepted 11 December 2022*)

Table S1. Comparison of adsorption capacity of some adsorbents for MB, CV, and RB 19

Dye	Adsorbent	q_m (mg/g)	Ref.
MB	Pine wood	3.99	[1]
	Pig manure	16.3	[1]
	Sludge derived biochar	29.85	[2]
	CMC-Alg/GO hydrogel beads	45.05	[3]
	Biochar derived from marine macroalgea	104	[2]
	CB-B	89.85	This study
CV	Almond shell	12.2	[4]
	Charred rice husk	62.85	[5]
	Bio-molecules composite with peanut hull waste	100.6	[6]
	Cellulose based on sugarcane bagasse	107.5	[7]
	CB-B	82.41	This study
RB 19	Coconut shell based activated carbon	4.104	[8]
	Biochar derived from *Eichhornia crassipes*	44.78	[9]
	Biochar derived from Coconut Shell	57.06	[10]
	Nano-Carbon adsorbent carbonized from small precursors	79.54	[11]
	Biochar derived from *Turbinaria*	92.5	[12]
	CB-B/Cs	304.49	This study

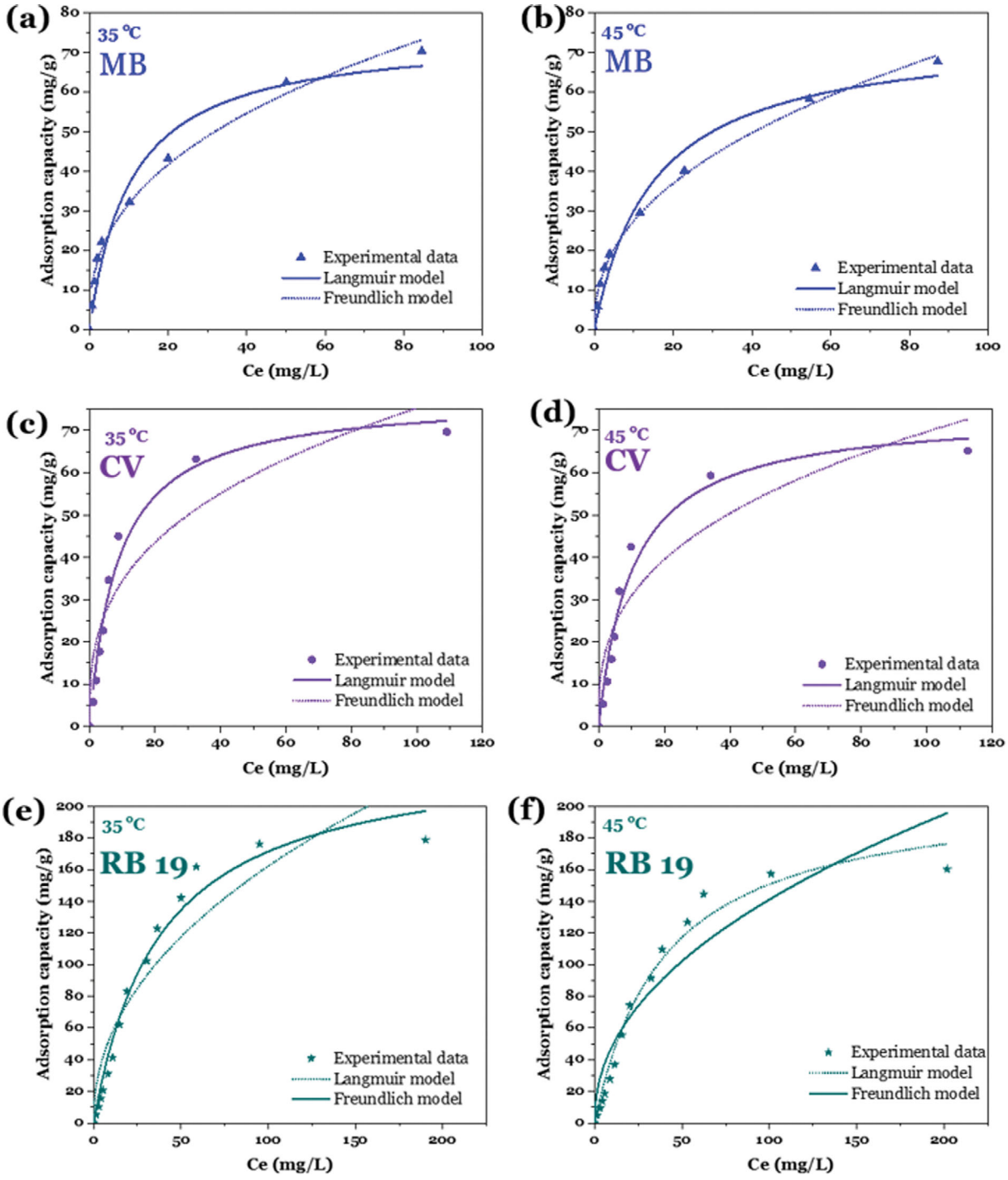

Fig. S1. Non-linear fitting of the Langmuir and Freundlich models for the adsorption of MB (a), (b), CV (c), (d), and RB 19 (e), (f) at 35 and 45 °C (c). Experiment conditions: pH=7, contact time of 20 min, temperature of 25 °C, adsorbent dosage of 4 g/L.

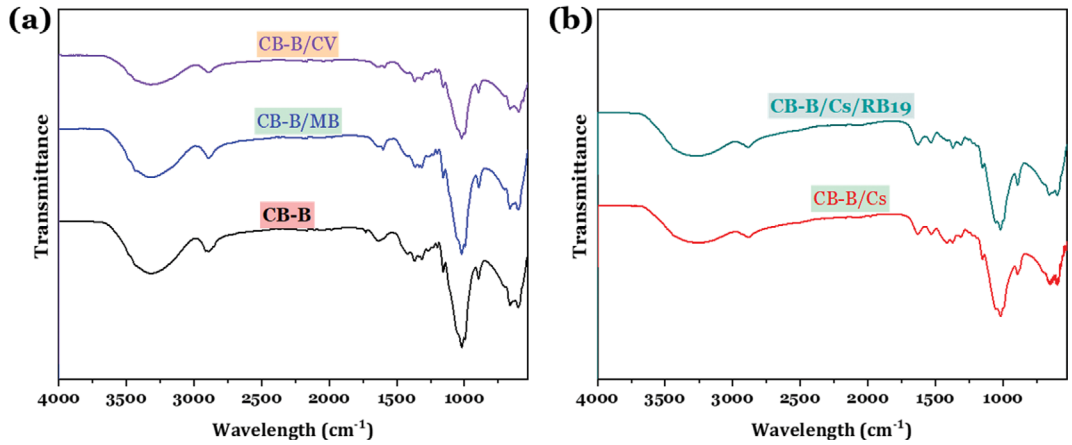

Fig. S2. (a) FTIR spectra of CB-B and (b) CB-B/Cs before and after adsorption.

REFERENCES

1. L. Lonappan, T. Rouissi, R. K. Das, S. K. Brar, A. A. Ramirez, M. Verma, R. Y. Surampalli and J. R. Valero, *Waste Manag.*, **49**, 537 (2016).
2. M. Parsa, M. Nourani, M. Baghdadi, M. Hosseinzadeh and M. Pejman, *J. Water Process Eng.*, **32**, 100942 (2019).
3. D. Allouss, Y. Essamlali, O. Amadine, A. Chakir and M. Zahouily, *RSC Adv.*, **9**, 37858 (2019).
4. I. Loulidi, F. Boukhlifi, M. Ouchabi, A. Amar, M. Jabri, A. Kali, S. Chraibi, C. Hadey and F. Aziz, *Sci. World J.*, **2020**, 5873521 (2020).
5. P. L. Homagai, R. Poudel, S. Poudel and A. Bhattarai, *Heliyon*, **8**, e09261 (2022).
6. N. Tahir, H. N. Bhatti, M. Iqbal and S. Noreen, *Int. J. Biol. Macromol.*, **94**, 210 (2017).
7. A. salah omer, G. A. El Naeem, A. I. Abd-Elhamid, O. O. M. Farahat, A. A. El-Bardan, H. M. A. Soliman and A. A. Nayl, *J. Mater. Res. Technol.*, **19**, 3241 (2022).
8. U. Isah A., G. Abdulraheem, S. Bala, S. Muhammad and M. Abdullahi, *Int. Biodeterior. Biodegrad.*, **102**, 265 (2015).
9. V. Dat Doan, T. Kieu Ngan Tran, A.-T. Nguyen, V. Anh Tran, T. Duy Nguyen and V. Thuan Le, *Environ. Nanotechnology, Monit. Manag.*, **16**, 100569 (2021).
10. R. Muralikrishnan and C. Jodhi, *ChemistrySelect*, **5**, 7734 (2020).
11. C. Liang, Q. Shi, J. Feng, J. Yao, H. Huang and X. Xie, *Nanomaterials*, **12**, 1814 (2022).
12. K. Vijayaraghavan and T. Ashokkumar, *Environ. Prog. Sustain. Energy*, **38**, 13143 (2019).